Reluctance Synchronous Machine with a Particular Cageless Segmental Rotor

I.A. Viorel[1], I. Husain[2], Ioana Chişu[1], H.C. Hedeşiu[1], G. Madescu[3] and L. Szabó[1]

[1] Dept. of Electrical Machines, Technical University of Cluj-Napoca
Daicoviciu 15, RO-3400 Cluj-Napoca, Romania
phone: +40 64 195 699 – fax: +40 64 192 055; e-mail: Ioan.Adrian.Viorel@mae.utcluj.ro

[2] University of Akron, Dept. of Electrical Engineering
Akron, OH 44325-3904, USA
e-mail: ihusain@uakron.edu

[3] Romanian Academy of Science, Timişoara Branch
Vasile Pârvan 17, RO-1900 Timişoara, Romania
e-mail: gmadescu@d109lin.utt.ro

Abstract —**Reluctance synchronous motor (RSM) can be an alternative to field oriented induction motor. The RSM's rotor topology is the key of the problem since an important saliency ratio leads to high power factor, torque/ampere and constant power speed range. This paper analyses a particular segmental rotor topology for a four pole RSM with concentrated nonmagnetic materials and flux barriers to reduce the q-axis flux. The field-computed parameters and performance are compared with tests.**

1. Introduction

The reluctance synchronous motor (RSM) is a singly salient machine. Its rotor is built up to employ the principle of reluctance torque to produce electromechanical energy conversion. As proved in previously published scientific works, good synthesises are given in [1], [2], RSMs are very attractive for line-start and variable speed electric drives. Their torque density, power factor and efficiency are competitive if the saliency ratio is high. The RSMs also offer fast torque and speed dynamics and wide speed range operation.

Almost all of the RSM's important performance parameters depends on the synchronous inductance ratio, or saliency ratio, $K=L_d/L_q$. The RSM's rotor is the most important key factor in obtaining the high saliency ratio. It emerged different RSM rotor constructions, the most important being [1]-[3]:

1. Segmental rotors
2. Rotors with flux guides and flux barriers
3. Axially laminated rotors

The literature consistently shows that the axially laminated rotors without starting cage produce the highest saliency ratio, [1]-[4]. The multiple barrier rotors with flux guides, which behaves almost as the axially laminated rotors, offer the possibility to achieve important saliency ratio too, (K=7÷11, [3]). Both these topologies imply quite complicated technology and high costs. Such a RSM may cost more than an equivalent induction motor (IM) and it should compensate the cost by its performances. There are a number of possible applications for RSM where the cost of the drive is of major importance. In such a case, a non-optimal structure may be chosen in favour of simpler and cheaper construction. From this point of view the rotor topology is the most important, since, as usually, the stator core is the same as for an induction motor and comes from a mass production, being of quite low cost.

The segmental and single flux barrier rotors are the simplest topologies for the cageless RSM, and they allow for a saliency ratio between 3.5 and 6, the greater values corresponding to large motors [2], [3]. The chosen topology was a segmental rotor with concentrated nonmagnetic material, Fig. 1.

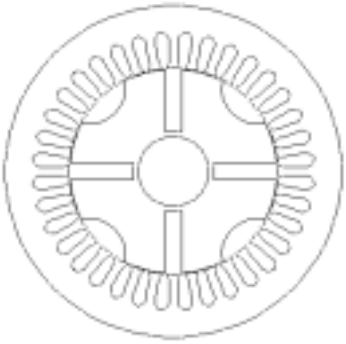

Fig. 1. Motor structure

Such a topology was previously proposed for a two pole RSM [5], but it implied technological difficulties, which can be partially avoided in the four pole case. The four pole rotor magnetic core was made of crude induction motor magnetic sheets manufactured to the actual topology. The prototype was built up using the stator core and the case of a 5.5 kW induction motor, the stator winding remaining unchanged. In the design stage different rotor topologies were considered. The chosen one allows for the highest saliency ratio with a less complicated structure and air-gap harmonics content.

The MagNet software package was used for 2D FEM analysis. The air-gap magnetic field harmonics content was analysed in different rotor positions and the motor's torque function of rotor position was computed, evincing quite important torque ripples. The prototype was examined on the test bench, mostly static measurements being performed due to the lack of a suitable vector controller. The test results were quite in good agreement with the computed ones. Considering the obtained results, a new prototype is built up by using the iron cores and the case of a four poles 2.2 kW induction motor. Minor changes in the rotor topology and technology were done, and the stator winding was adequately designed.

2. Rotor topology

Taking into account the results obtained in [5] and the technological difficulties, which the two pole rotor implies, the solution considered was quite the same, but for a four poles motor. Basically, the solution remains a segmental rotor with concentrated nonmagnetic material, Fig.1.

In the designing stage, many variants were tested via 2D FEM magnetic field computation. The stator remains unchanged since it is an induction motor stator with 36 slots and a double layer winding.

In Fig. 2 the flux plots on the *d* and *q*-axis are presented for some of the variants, the phase current being 12.4 A.

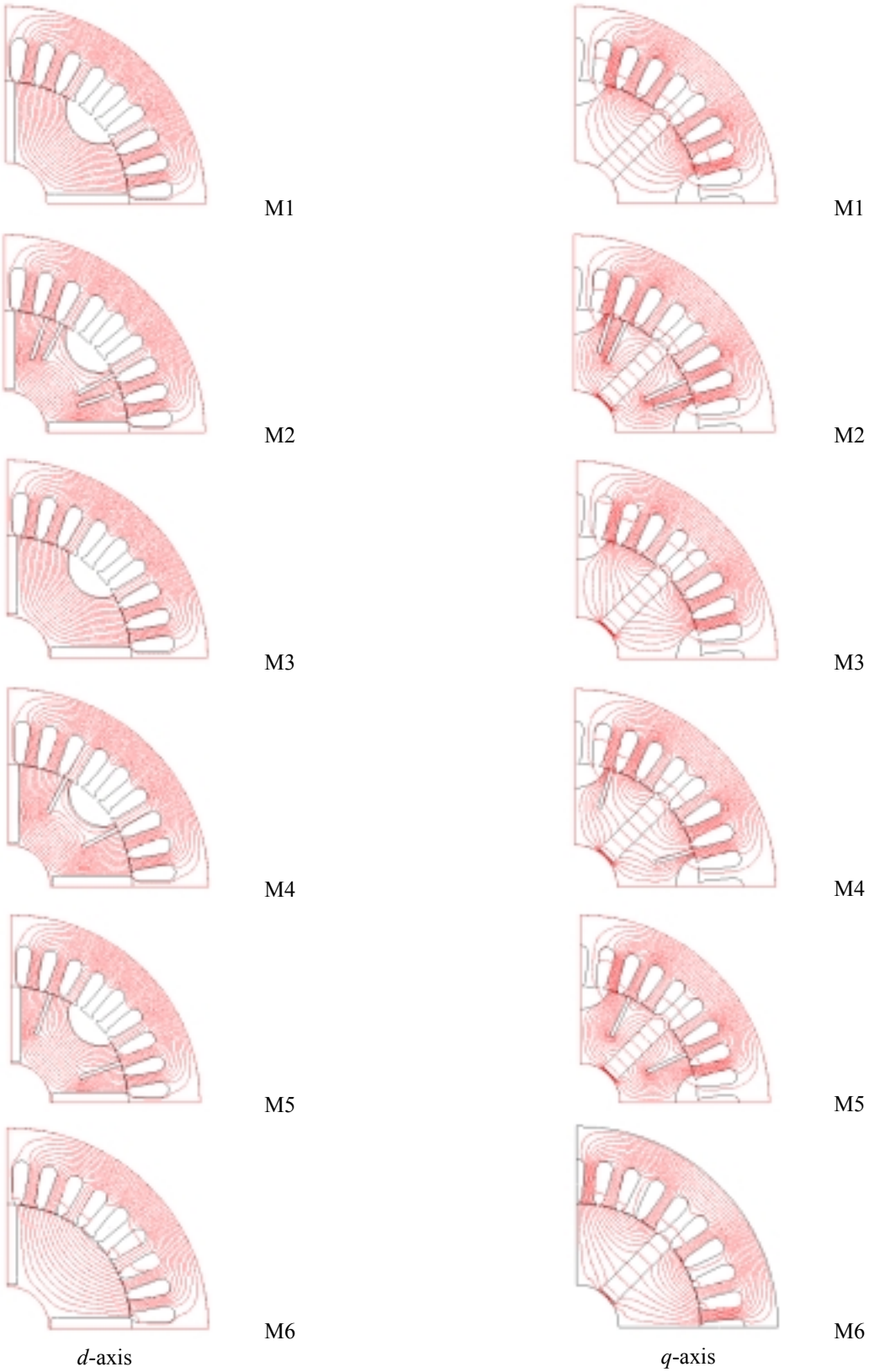

Fig. 2. The *d*- and *q*-axis flux plots for M1-M6 rotor variants

All the variants given in Fig. 2 have the concentrated nonmagnetic material on the rotor *d*-axis with a width of 10 mm and the semicircular slot with the minimum radius on the q-axis. The ideal variant, M1, has no core bridge between the rotor segments and no flux barriers.

For variants M2-M5, given in Fig. 2, the semicircular slot has the same radius, but there is a 2 mm core bridge between rotor segments. For M2 variant two radial flux barriers were considered since M4 and M5 have respectively only one of the barriers. The M3 variant is identical to M1 one, but it has core bridge between rotor segments. The M6 variant has no flux barriers or semicircular slot.

The values of the magnetising inductances, M_d, M_q, the saliency ratio $K=M_d/M_q$, the electromagnetic torque T, and efficiency η for M1-M6 variants computed via the 2D FEM analysis, are given in Table I.

TABLE I

	M_d [mH]	M_q [mH]	K	T [Nm]	η
M1	116,329	19,866	5.855	19.3	0.735
M2	109,893	27,143	4.048	18.0	0.721
M3	116,323	28,050	4.146	19.4	0.736
M4	112,945	27,486	4.109	18.7	0.728
M5	113,502	27,748	4.090	18.8	0.729
M6	124.374	33.048	3.763	20.9	0.750

The electromagnetic torque is:

$$T = p(L_d - L_q) I_d^2 \frac{1}{k} \tag{1}$$

where

$$k = \frac{I_d}{I_q} = \frac{\lambda_d}{\lambda_q} \frac{L_q}{L_d} \tag{2}$$

and the synchronous inductances are

$$L_d = M_d + L_{s\sigma}\,; L_q = M_q + L_{s\sigma} \tag{3}$$

$L_{S\sigma}$ being the stator phase leakage inductance.

The efficiency comes as:

$$\eta = \frac{P_2}{P_2 + \Sigma p} \cong \frac{T\Omega_s}{T\Omega_s + \Sigma p} \tag{4}$$

where

$$\Omega_s = 2\pi n_s = 157.08 \text{ rad/sec}$$

$$\Sigma p = p_{js} + p_{Fe} + p_m$$

$$p_{js} = 3R_s \cdot I_s^2$$

The iron core losses, p_{Fe}, and the mechanical losses, p_m, were taken equal to the computed losses of the corresponding induction motor,

$$p_{Fe} = 205 \text{ W},\ p_m = 22 \text{ W}$$

The stator phase leakage inductance $L_{S\sigma}$ is computed as usually [6], the value, which includes the end winding leakage, being $L_{S\sigma}$=8.5256 mH.

The parameters to vary in order to obtain the different rotor variants analysed via 2D FEM were: the nonmagnetic material width (2 mm step being considered) the radius of the semicircular slot, and the depth of the radial flux barriers. As one can see, the influence of the flux barriers is not useful since the presence of the flux barrier slightly decreases the *q*-axis magnetising inductance, but reduces more the *d*-axis magnetising inductance. The semicircular hole on the *q*-axis does not lead to an important saliency ratio increase, but this hole had to be kept due to technological reasons since the rotor structure is consolidated with four insulated nonmagnetic bars placed in that holes. The bars are belted together with special rings, made of nonmagnetic insulated material, fixed on the shaft outside the rotor's stack.

The core bridge between the rotor segments does not affect the *d*-axis magnetising inductance, as one can see comparing the M1 and M3 models. The *q*-axis magnetising inductance is increased with 34% and consequently decreases the saliency ratio *K*. The rotor shaft is of nonmagnetic material and it was adequately considered in the 2D FEM model.

The new, under construction, prototype has no semicircular holes on the rotor *q*-axes and the rotor segments consolidation is solved, technological, in a different way. For this prototype, the stator winding is adequately designed and the motor will be fed by a fully controlled frequency converter.

The harmonic content of the air-gap field is quite important and it can be seen from the harmonic analysis done on the *d*- and *q*-axis air-gap field for the M3 model, shown in Fig. 3 and Fig. 4.

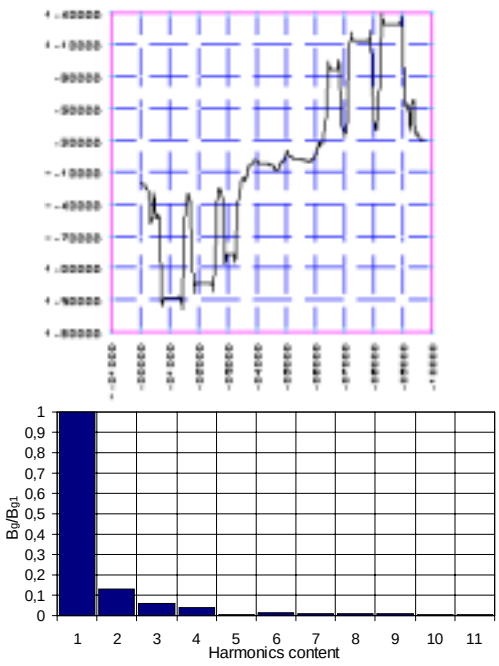

Fig. 3. The air-gap flux density variation on a pole pitch and the corresponding harmonic spectrum for *d*-axis

In Fig. 3 the air-gap flux density variation on a pole pitch and the corresponding harmonic analysis is shown for the case of the stator MMF oriented on the rotor *d*-axis direction. Fig. 4 shows the same curves, but for the case of the stator MMF oriented on the *q*-axis direction. The harmonics content is greater in this last case, and the presence of the flux barriers increases the harmonics content on both axes.

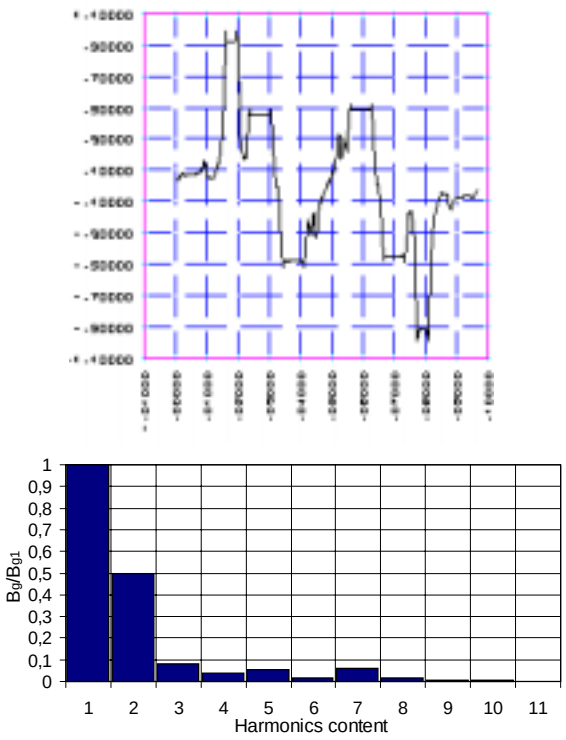

Fig. 4. The air-gap flux density variation on a pole pitch and the corresponding harmonic spectrum for *q*-axis

In Fig. 5 the electromagnetic torque variation function of the rotor position is shown for the M3 model, when the phase current is 12.4 A.

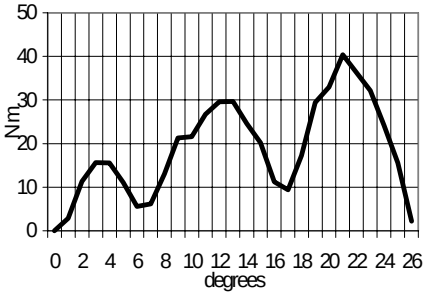

Fig. 5. The electromagnetic torque variation function of the rotor position

As one can see, the torque varies importantly with the rotor position, the flux barriers and the semicircular hole on the rotor *q*-axis, producing an increase in the torque variation. The torque ripple decreases when the rotor has no circular hole on the *q*-axis. In the paper were presented only the results obtained for M3 model since this was the topology adopted for he manufactured machine.

3. Results and conclusions

The four poles RSM was manufactured on a 5,5 kW induction motor frame with the main dimensions:

- stator interior diameter D_{si}= 0.124 m
- stator exterior diameter D_{se}= 0.2 m
- stack length l_s=0.12 m
- air-gap length g= 0.45·10^{-3} m

The case and the stator remain unchanged. The stator winding is a full pitch double layer one with 204 turns per phase. The rotor core is made of crude induction machine magnetic sheets, manufactured to the actual topology by electroerosion. Since there are 2 mm iron bridges between the rotor segments, the rotor sheets stay together on the stator shaft. The rotor structure is consolidated with four insulated bars placed in the semicircular holes and belted together with two special rings fixed on the shaft. The manufacturing technology is quite complicated, therefore for the new prototype, under construction, some changes were made.

All the inductances, including the phase magnetising inductance were computed via the usual way, [6]-[7], for the basic squirrel cage induction motor. The obtained values are:

- Induction motor phase magnetising inductance M= 0.209 H
- Carter's factor k_c=1.2485
- Saturation factor k_s= 1.4
- Equivalent air-gap g_e=0.7866 mm
- Stator phase slot leakage inductance $L_{s\sigma s}$=3.4256mH
- Stator phase end winding leakage inductance $L_{s\sigma c}$=5.1mH
- Stator phase leakage inductance $L_{s\sigma}$=8.5256mH
- M_d/M ratio of the M_3 model k_d=0.608

The stator phase leakage inductance was measured before to place the rotor inside the stator. The results of measurements are given in Table II.

TABLE II

U [V]	I [A]	P [W]	R_s [Ω]	$X_{s\sigma}$ [Ω]
17.32	5.62	27.7	0.876	2.955
23.09	7.69	52.0	0.879	2.871
28.87	9.64	79.7	0.857	2.869

The average phase leakage reactance is $Xs\sigma$=2.898 Ω which leads to an average phase leakage inductance $L_{s\sigma}$=9.23 mH. It means 7.6 % more than obtained by analytical computation, which is fearly good.

The synchronous inductances, L_d, and L_q were obtained by employing different testing procedures [4], [8]:

i) No loaded test (L_d, Table III)
ii) Locked rotor, one phase fed with AC (L_d and L_q, Table IV)
iii) Standstill current decay test [2], [8] (the values L_d=0.1226 H, L_q=0.0358 H were obtained at the initial DC current i_0=5 A)

TABLE III

U [V]	I [A]	P [W]	X_d [Ω]	L_d [H]	pf.
125	2.95	150	38.709	0.1233	0.407
150	3.55	216	38.002	0.121	0.406
220	5.24	462	38.463	0.1225	0.401

TABLE IV

U [V]	I [A]	P [W]	X [Ω]	L [H]	Axis
77.20	2.00	22.0	38.206	0.1217	d
102.15	2.66	39.7	37.99	0.121	d
78.0	6.8	159.5	10.94	0.0348	q
95.2	8.21	240.0	11.04	0.0351	q

At no load test, since the motor was fed from the net at 50Hz, the rotor was brought to the synchronous speed with a smaller auxiliary DC motor, which was decoupled after synchronising the RSM.

In Table V the average values obtained by tests are given (not only that given above) in comparison with computed values for the M3 model.

TABLE V

COMPUTED					TESTS					
2D FEM		Analytical			No load	One phase supplied		SSCD		$L_{s\sigma}$
M_d	M_q	M	K_d	$L_{s\sigma}$	L_d	L_d	L_q	L_d	L_q	
116.32	28.05	209	0.608	8.526	122.3	121.6	35.0	122.6	35.8	9.23

In table V all the inductance's values are given in mH. As one can see, the test's results are quite in good agreement with the computed values.

At no load the computed current is:

$$I_d = \frac{\sqrt{3}*U_s}{X_{dm}+X_d} = \frac{\sqrt{3}*220}{36.52+39.2} = 5.03A$$

compared with the measured one of 5.24 A.

The power factor obtained at no load test for the original four poles 5.5 kW induction motor is 0.189, compared with 0.401 in the case of RSM fed from the net. Since the DC machine, employed as starter and breaker, had a smaller power, the load tests went up to 2.5 kW output power, the efficiency variation function of output power being shown in Fig. 6.

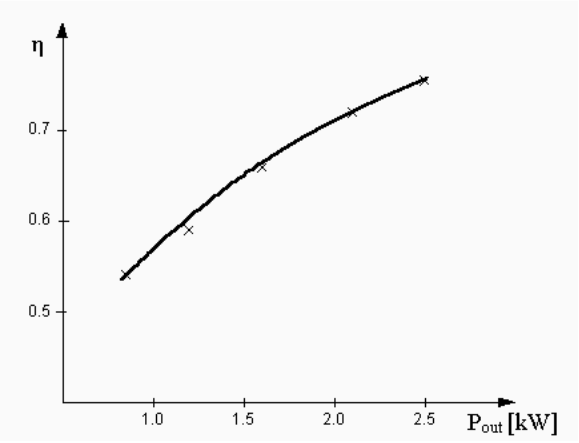

Fig. 6. Efficiency versus output power

The maximum achieved efficiency is 0.748, compared with the 0.736 value computed and given in Table I in the case of the net fed RSM.

In order to evaluate the air-gap flux density harmonics content a simple test set-up was proposed. In Fig. 7 is presented the set-up when the MMF axis coincides with the rotor *d*-axis.

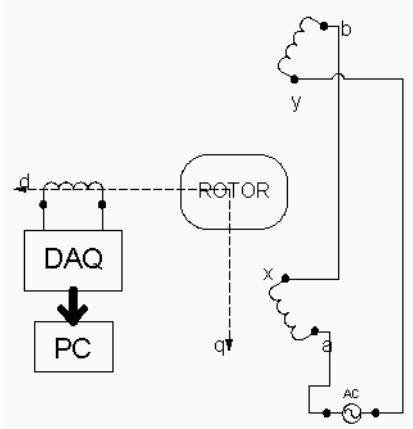

Fig. 7. Test set-up to evaluate the harmonics

The 50 Hz voltage source was applied between the phase *a* and *b* terminals, with the phases connected as to produce a resultant MMF on the same direction with the phase *c* axis. The phase *c* induced voltage is containing the same harmonics as the air-gap field does. The phase *c* EMF is acquired with a data acquisition card by using the LabVIEW environment. The harmonics content, when the produced MMF is on the rotor *d*-axis, the same with phase *c* axis, is given in Fig. 8.

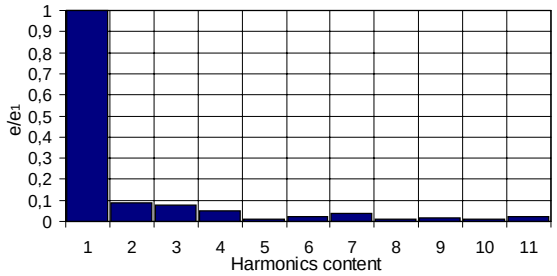

Fig. 8. Phase *c* EMF harmonics content on the rotor d-axis

It results quite the same harmonics content as that computed from the flux density distribution on the rotor *d*-axis, Fig. 3.

Due to the lack of a vector controlled electronic converter the RSM was fed only from the net at constant frequency and the obtained results concerning the efficiency and power factor are not relevant. Anyway the RSM motor behaves almost as well as the original induction one and that is favorable. It is clear that the RSM can deliver more torque at low speed within the same thermal rating since the losses are smaller. The segmental rotor topology proposed in this paper is not capable of achieving a larger saliency ratio than 4 at full load, quite the same value which can be obtained with the single barrier topology [3]. The harmonics content is not that high for the segmental rotor RSM, as for the single barrier one, and so are the component of torque ripple owning to the combination of rotor saliency and stator slotting. The manufacturing technology for the segmental rotor RSM proposed is the simplest, and consequently the cheapest possible.

The tests obtained values are in good agreement with the computed ones, and that is very important from the designing point of view. It means that for the future the 2D FEM computation combined with the analytical calculation for the leakage can be employed entirely up to find an optimum variant. The optimum variant should have a saliency ratio as large as possible, but with a low component of torque ripple and flux density harmonics content.

The overall conclusion is that the segmental rotor topology proposed here is a very simple one, and allows for achieving quite good performance, the ratio cost / performance being a very good one.

Acknowledgement

This work was supported by the Romanian Science Council.

The authors are grateful also to Electromotor S.A. from Timişoara, Romania which fabricated the experimental reluctance synchronous motor.

References

[1] I. Boldea, *Reluctance synchronous machines and drives*, Clarendon Press, Oxford (1996).

[2] G. Henneberger, I.A. Viorel, *Variable reluctance electrical machines*, Shaker Verlag, Aachen (2001).

[3] D.A. Staton, T.J.E. Miller, S.E. Wood, "Maximising the saliency ratio of the synchronous reluctance motor", *IEE Proc.-B,* Vol. 140, No. 4, pp. 249-259, July 1993.

[4] T. Matsuo, T.A. Lipo, "Rotor design optimization of synchronous reluctance machine", *IEEE Transactions on Energy Conversion*, Vol. 9, No. 2, pp. 359-365, June 1994.

[5] Ioana Chişu, K.A. Biro, I.A. Viorel, H.C. Hedeşiu, R.C. Ciorba, "On the synchronous reluctance machine rotor geometry", in *Proc. Electromotion 1999*, Vol. 1, pp. 161-166.

[6] B.J. Chalmers, A. Williamson, *AC machines electro-magnetics and design*, John Wiley and Sons Inc., New York (1991).

[7] A. Vagati, M. Passtorelli, G. Franceschini, S.C. Petrache, "Design of low-torque-ripple synchronous reluctance motors", *IEEE Transactions on Industry Applications*, Vol. 34, No. 4, pp. 754-765, 1998.

[8] Valeria Hrabovcova, M. Licko, L. Janousek, P. Rafajdus, J. Mihok, "Methods of determination of the cage-rotor reluctance synchronous motor parameters and their comparison", in *Proc. of Electromotion 1999*, Vol. 1, pp. 131-136